Bulletin of the Seismological Society of America, Vol. 103, No. 2A, pp. 1154–1164, April 2013, doi: 10.1785/0120110245

Ⓔ

*Short Note*

# Near-Surface Shear-Wave Velocity Structure of the Chiayi Area, Taiwan

by Cheng-Feng Wu and Huey-Chu Huang

**Abstract** This paper uses microtremor-array measurements to obtain an overall view of *S*-wave velocity structure in the Chiayi area, Taiwan. The Rayleigh-wave dispersion curves are calculated using the frequency-wavenumber ($f$-$k$) spectrum method and then the *S*-wave velocity structure of the area is estimated by surface-wave inversion. According to the inversion results, the *S*-wave velocities decrease from east to west. If the *S*-wave velocity of the bedrock is assumed to be 1500 m/s, the depths of the alluvium are between 560 and 1400 m gradually increasing from east to west. In order to understand the variations of the shallow *S*-wave velocity in the area, we sketch 2D and 3D maps using the imaging techniques based on interpolation algorithms. From the 3D results, the thickness of the sediments having an *S*-wave velocity in the range 270–1500 m/s increases from east to west; whereas the thickness of the layers having an *S*-wave velocity in the range 1500–2370 m/s decreases from east to west. The results are also in good agreement with the geological and geophysical information of the Chiayi area. Therefore, microtremor-array measurement provides a good alternate to estimate shallow *S*-wave velocity structure.

*Online Material:* Figures showing observed and calculated phase velocities, $f$-$k$ spectra, dispersion curves, inverted velocity models, sensitivity kernels, and $V_S$ contour maps and electric resistivity maps.

## Introduction

The 22 October 1999 Chiayi earthquake ($M_L$ 6.4) occurred near Chiayi City and destroyed some local buildings. In addition, over 20 destructive earthquakes have occurred in or near the Chianan area from 1896 to 2007. These earthquakes have killed ~2000 people and destroyed ~27,200 houses (Chang, 2008). As is well known, alluvial sediments often come from fluvial processes, which consist of mineral weathering, erosion, and deposition on surface materials. Because such sediments are poorly cemented and unconsolidated, the safety of buildings is strongly affected by such subsurface *S*-wave velocity structures during earthquakes. Moreover, two-thirds of the Chiayi area is made up of alluvial strata; therefore, understanding the overall *S*-wave velocity structure of this area is important in seismic-hazard assessment and ground-motion prediction.

$V_S$ data are now largely obtained using well-logging methods, which are time-consuming and costly. Compared to direct borehole methods, non-intrusive surface methods to obtain $V_S$ information are considerably less expensive. Besides, the conventional reflection and refraction exploration methods are appropriate for estimating deep *P*-wave velocity structure rather than *S*-wave velocity structure because artificial *S*-wave sources still face problems regarding their energy, reliability, and practicability, especially for exploration of deep sedimentary layers. Therefore, compared with other methods, microtremor-array measurement has several advantages (Horike, 1985): (1) it can be observed at any time and location; (2) observation is much easier than with other exploration methods; (3) it causes no environmental problems; (4) geological conditions down to a depth of more than 100 m can be inverted, as far as microtremors of required frequency range are observed. As an economical and practical substitute, microtremor measurement is appropriate for estimating the $V_S$ structure.

*S*-wave velocity structure plays an important role in site effects. A number of studies have derived near-surface material properties from microtremor-array measurements. Satoh *et al.* (2001) estimated phase velocities of microtremors in the frequency range from 0.5 to 3 Hz using the frequency-wavenumber ($f$-$k$) spectrum method (Capon, 1969) and succeeded in obtaining the *S*-wave velocity structures for depths of up to 1.1 km at six sites using the Rayleigh-wave inversions in the Sendai basin, Japan. Similarly, Dutta *et al.* (2007) inverted 1D *S*-wave velocity structures using the stochastic inversion technique (Herrmann, 1987) beneath nine sites in Anchorage, Alaska. To investigate the spatial variations of

*S*-wave velocity at different depths (20–500 m) in the basin, they used 2D interpolation of *S*-wave velocity structures. There are some studies that discussed site characterization by combining the results from array- and single-station microtremor measurements. The resulting dispersion curves were used together with the horizontal-to-vertical (H/V) curve in a joint inversion scheme for the estimation of the *S*-wave velocity profiles in Istanbul, Turkey (Picozzi *et al.*, 2009). Analogously, the array- and single-station microtremor measurements were carried out at 3 and 116 sites, respectively, by Mundepi *et al.* (2010) around the city of Delhi, India. Combining the information provided for both methods, they characterized the soil sediments of the city, obtaining different zones of resonance frequency, soil thickness, and mean *S*-wave velocity. In order to determine a high-resolution 3D velocity structure for a 26 km × 12 km area in the northern part of the basin of Santiago de Chile, Pilz *et al.* (2010) analyzed microtremor recordings at 125 sites for deriving the H/V spectral ratios and used additional geological and geophysical constraints in the inversion procedure. The final 3D *S*-wave velocity model was derived by interpolation with a kriging technique between the single velocity profiles. Moreover, Pilz *et al.* (2011) applied the relationship between the *S*-wave velocity and depth from Pilz *et al.* (2010) to construct the 3D mesh and simulated the strong ground motion within the Santiago de Chile Metropolitan area using the 3D spectral element method.

There have been earlier studies to determine laterally varying velocity structures in the crust of the Chianan area, Taiwan. Chung and Yeh (1997) used short period Rayleigh-wave dispersion data to obtain a velocity model beneath the strong-motion network in southwestern Taiwan. They resolved clear lateral variation in *S*-wave velocity along a cross section perpendicular to the western structural grain proposed by Ho (1982). To further investigate lateral variations in *S*-wave velocity structure up to a depth of 8 km under southwestern Taiwan, Hwang *et al.* (2003) used fundamental-mode Rayleigh waves with periods of 1.1–5.5 s. According to velocity structure inversions, this region has obvious lateral velocity variations that systematically increase from west to east. On the whole, *S*-wave velocity in the Western Foothills is higher than that of the Western Coastal Plain and there is a large velocity variation at shallow depth in the Western Foothills. Wen and Chen (2004) investigated $V_P$ structures and $V_P/V_S$ ratios of the crust and upper mantle beneath the Chianan area by adopting a damping least-squares inversion method. They indicated that variations in velocity structure beneath the Chianan area were caused by local geological structures, fault crossing, and the existence of the Pei-Kang High area. Huang and Wu (2006) studied shallow *S*-wave velocity structures (0–1.5 km) in Chiayi City using the microtremor records of seven sites. Lin *et al.* (2009) estimated shallow *S*-wave velocity structures (0–3 km) using array measurements of microtremors at seven sites in the Western Coastal Plain of Taiwan. The sites from north to south included: Lugang, Erlin, Huwei, Dongshih, Taibao, Yijhu, and Jiali, which are spread for ~100 km across four counties. Although the above studies provided velocity structures of the crust beneath the Chiayi and Tainan areas, the overall shallow *S*-wave velocity structure of the Chiayi area is still not clear. However, this knowledge is very important for understanding site effects and providing ground-motion prediction. Therefore, in this study, we conduct microtremor-array measurements at 46 sites to explore shallow *S*-wave velocity structures in the Chiayi area. In order to examine the validity of the *S*-wave velocity structures estimated from microtremor-array measurements, we compare the results with those from the geological and geophysical data.

## Sites and Data

The Chiayi area is located in Taiwan's southwest (Fig. 1a). Topographically, the area includes the Chianan plain (part of the Western Coastal Plain) and the Chiayi hills (part of the Western Foothills). The western and central parts of this area are on the alluvial plain whereas the eastern part is on the hill. The area's drainage system from top to bottom is composed of the Peikang, Puzih, and Bajhang Rivers, and they predominantly flow east to west. The Chiayi hills are located on the western side of the Western Foothills, and the strata of the Chiayi hills are composed mainly of rocks with ages ranging from the Pliocene to Pleistocene. The Chianan plain is part of the Western Coastal Plain and it includes tidal flats and marine cut terraces near the seashore. It is a young coastal plain that is still undergoing uplift. It continuously expands westward through the rapid deposition of sediments and regional uplift. Rivers flow rapidly through the Chianan plain bringing large amounts of discharge and generating extensive floodplains that provide fertile soils for agricultural production in Taiwan (Chang, 2008).

In order to study the shallow *S*-wave velocity structures of the Chiayi area, we conduct microtremor-array measurements at 46 sites (Fig. 1b). The *S*-wave velocity structures at seven sites: CBA, CHG, CIH, CWB, SGA, SHP, and YRU in Chiayi City were estimated by Huang and Wu (2006) and are re-estimated in this study. Most of the measuring sites are located on the plain on recent alluvial deposits; however, some measurements are taken from sites over rocky outcrops that may be extensions of the western region of the Chiayi hills. Microtremor arrays of four different sizes (*S*, *M*, *L*, and *X*) are measured at each site. Figure 2 shows the array configurations in both the *S* and *X* sizes for site WET, as an example. The center station at each site is common for *S*(radius = 50 m), *M*(radius = 100 m), *L*(radius = 200 m), and *X*(radius = 400 m) arrays. We deploy seven stations in the form of two different aperture triangles around the center station at each array. To avoid possible low-frequency disturbances induced by wind and structures, the sensors are covered with flowerpots during measurements and placed as far as possible from buildings and trees. At each site, microtremor data is continuously recorded during day time for 68 minutes at a sampling rate of 200 Hz. The microtremor data are recorded by 24-bit digital recorders (SAMTAC-801B), and each recorder con-

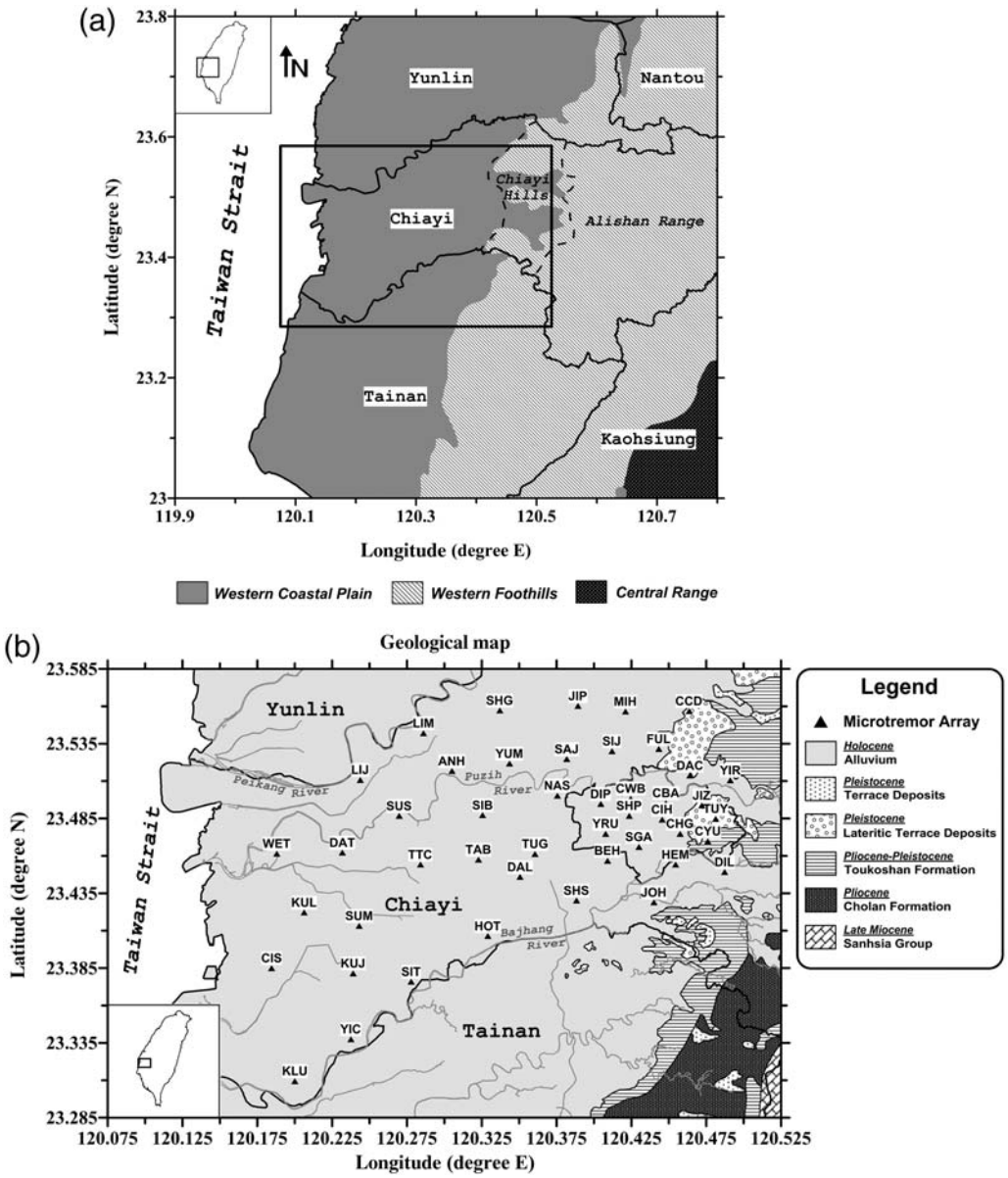


**Figure 1.** (a) Geological sketch of southwestern Taiwan. Two main units are the Western Coastal Plain and the Western Foothills. Rectangle represents the Chiayi area studied here. (b) Geological map of Chiayi area superimposed with the 46 used sites (solid triangles). The gray lines denote distributions of the principal rivers, which flow mainly along the east–west direction in this area. The closed and thick black lines within the study area are the boundary of Chiayi City (modified from the Central Geology Survey, 2010).

nects to a tri-axial-servo velocity sensor (VSE-315D). This velocity sensor has a flat amplitude response from 0.1 to 70 Hz. The records are synchronized by the Global Positioning System (GPS) for each measurement with a timing accuracy for GPS correction of within 1 ms. The positions of the sensors are determined using a GPS Pathfinder Pro XRS differential receiver that provides real-time sub-meter accuracy.

## Methods of Analysis

### $f$-$k$ Spectral Analysis Method

The technique used in this study for data analysis is the maximum likelihood method (MLM) proposed by Capon (1969). This method uses the cross-power spectral densities of an array of $N$ sensors to estimate the $f$-$k$ spectrum, refining it with coherency estimates. The estimate of the $f$-$k$ spectrum $P(f,k)$ by MLM is given by

$$P(f,k) = \left[\sum_{i,j=1}^{N} \phi_{ij}^{-1}(f)\exp(i\vec{k}\cdot\vec{r}_{ij})\right]^{-1}, \qquad (1)$$

in which $N$ is the number of sensors; $\phi_{ij}(f)$ is the cross-power spectrum between the $i$th and $j$th sensors at frequency $f$; $\vec{r}_{ij} = \vec{r}_j - \vec{r}_i$ for which $\vec{r}_i$ and $\vec{r}_j$ are the position vectors of the $i$th and $j$th sensors, respectively; and $\phi_{ij}^{-1}(f)$ is the element of the corresponding inverse for the matrix $\phi_{ij}(f)$.

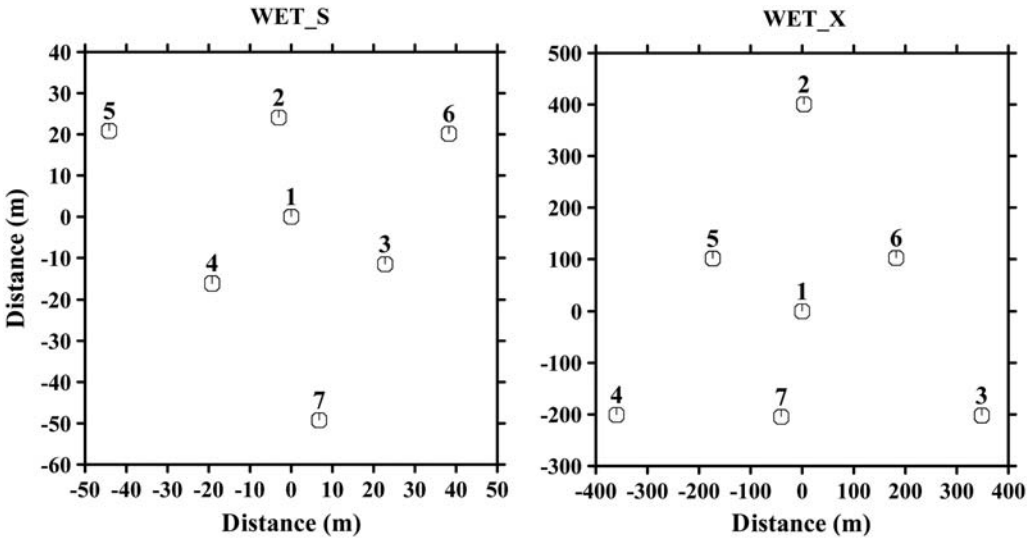


**Figure 2.** The geometries of the *S* and *X* arrays at site WET.

Based on the results of the *f-k* power spectrum, the phase velocity $V$ can be estimated by

$$V = f/\sqrt{k_{x_0}^2 + k_{y_0}^2}, \tag{2}$$

in which $k_{x_0}$ and $k_{y_0}$ correspond to the peak power positions in the wavenumber space.

### Inversion of the Velocity Structure

The relationship between the dispersion curve of the surface wave and the velocity structure is nonlinear. For convenience in structure inversion, a quasi-linear relationship between the dispersion curve and velocity structure is retrieved through a Taylor-series expansion with high-order terms being neglected. Because the phase velocities are more sensitive to the *S*-wave velocity structure than to the *P*-wave velocity and density structures (Horike, 1985), only the *S*-wave velocity is inverted in this study. The formula, joining the dispersion curve and velocity-model parameters, can be written as follows (Hwang *et al.*, 2003):

$$\Delta C(T_j) = \sum_{i=1}^{N} \left( \frac{\partial C(T_j)}{\partial \beta_i} \right) \Delta \beta_i, \tag{3}$$

in which $\Delta C(T_j)$ is the difference between the observed and the predicted phase velocity derived from the initial velocity model at the $j$th period ($T_j$); $N$ is the number of layers; $\partial C(T_j)/\partial \beta_i$ is the partial derivative of the phase velocity of the $j$th period with respect to the *S*-wave velocity of the $i$th layer; and $\Delta \beta_i$ is the resulting difference in the *S*-wave velocity of the $i$th layer between adjacent inversions.

To solve model parameters ($\Delta \beta_i$) of equation (3), we employ a surface-wave inversion program based on damped least-squares and developed by Herrmann (1991). Moreover, the program used here is based on the assumption that the fundamental mode of Rayleigh wave is dominant. Smoothing constraints, the difference between adjacent model parameters as an approximation of a derivative to control solution roughness, are also used (e.g., Menke, 1984). In this study, an initial layered model at each site is first constructed with assigned values of thickness, *S*-wave velocities, and Poisson's ratio for each layer. For this initial model, we take a half-space structure with *S*-wave velocity being the maximum phase velocity divided by 0.92 at the used lowest frequency as *S*-wave velocity in the initial model. If we are using a maximum frequency of 5 Hz, and assuming a phase velocity of ~300 m/s, the minimum expected wavelength is 60 m. According, by rule-of-thumb calculation, the highest resolution of thickness can be estimated as being about one-third of the observed minimum wavelength (e.g., Asten and Henstridge, 1984). Therefore, we expect to resolve a 20-m-thick layer. Similarly, the depth resolution of the available data is limited by the minimum frequency and its corresponding phase velocity. In addition, the total layer number and the damping value adopted are 80 and 1.0, respectively, for the inversion. The inversion process will be terminated when the difference in *S*-wave velocity for each layer between the adjacent inversions is less than 0.001 km/s. Although a good agreement does not ensure the uniqueness of the solution, it does indicate rationally the point for which theoretical phase velocities from inverted *S*-wave velocities agree well with observed phase velocities. Finally, these combined methods allow for a reasonable velocity model to be obtained.

## Results and Discussions

### *f-k* Analysis of Microtremor-Array Data

Because contaminated blocks (i.e., non-stationary signals) due to artificial noises are excluded from observation

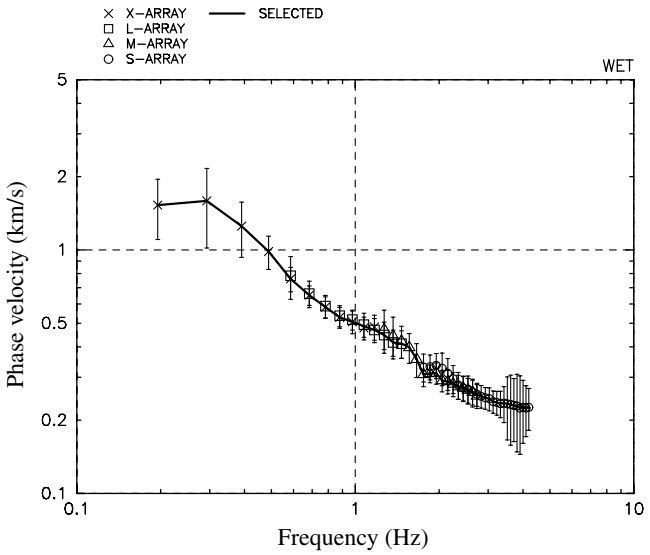


**Figure 3.** Average and average ±1 standard deviations of the phase velocities we obtain from the recordings at WET. The different symbols represent the results from the arrays of different size. The black line is the final phase velocity that we select in this study.

records, we are able to estimate phase velocities using $f$-$k$ spectral analysis based on the MLM (Capon, 1969). Each observed vertical-component record is divided into time segments of length 20.48 s for the $S$ and $M$ arrays and 40.96 s for the $L$ and $X$ arrays by overlapping one-half of each window length. The maximum wavenumber for each $f$-$k$ spectrum is set by effective Nyquist wavenumber, which refers to the reciprocal of twice the minimum station separation.

Phase velocity can be estimated from the frequency and the wavenumber of the maximum peak in the $f$-$k$ spectrum. Because the phase velocity of the Rayleigh wave is less than the $S$-wave velocity, we set the upper threshold of the phase velocity as 4.5 km/s. Moreover, we also search for maximum ($C_{\max}$) and minimum ($C_{\min}$) phase velocities for each frequency and exclude unreliable phase velocities with a significance level of 5% of ($C_{\max} - C_{\min}$). Then, we choose a value by taking the average of the reliable phase velocities.

The average and average ±1 standard deviations of the phase velocities obtained from the recordings at site WET are shown in Figure 3. The different symbols represent the results from the arrays of different size. The final phase velocities (the solid line in Fig. 3) are chosen by following the sequence of the $X$(0.2 Hz ≤ $f$ < 1.1 Hz), $L$(1.1 Hz ≤ $f$ < 1.6 Hz), $M$(1.6 Hz ≤ $f$ < 2.7 Hz), and $S$ arrays (2.7 Hz ≤ $f$ < 4.2 Hz) from low frequencies to high frequencies. Basically, the results of the $X$ and $L$ arrays are stable at lower frequencies, whereas those of the $S$ and $M$ arrays are stable at higher frequencies. Figure 4 represents the dispersion curves of phase velocities obtained from the recordings observed at all the arrays of the 46 sites. Comparatively, the estimated phase velocities vary from site to site.

## Inversion of the *S*-Wave Velocity Structures

We first invert $S$-wave velocity structures using the differential inversion technique (Herrmann, 1991). Based on Figure 3, the shallow $S$-wave velocity structure at site WET is shown in Figure 5a. During the inversion analysis, the higher modes of Rayleigh wave have been neglected (Ⓔ Figs. S1–S3 in the electronic supplement). Besides, the uncertainties of the phase velocities have not been included here (see Ⓔ Fig. S4, electronic supplement). In order to demonstrate the validity of the inverted velocity structure, we compare the theoretical phase velocities of the fundamental mode of the Rayleigh wave for the inverted structure (solid line) with the observed phase velocities (open circles) in Figure 5b. The dashed line represents the initial model for the inversion. We take a half-space structure with an $S$-wave velocity that is the maximum phase velocity divided by 0.92 at the used lower frequency as the $S$-wave velocity in the initial model (see Ⓔ Figs. S5 and S6, electronic supplement). Obviously, they match well.

Based on phase-velocity dispersion curves (Fig. 4), Figure 6 displays the $S$-wave velocity structures at all sites inverted using differential inversion technique. Owing to depth resolution being limited by minimum frequency and its corresponding phase velocity, the $S$-wave velocity structures at some sites cannot reach a depth of 2000 m. In order to clarify the resolution of the $S$-wave velocity model, we calculate the resolving kernel/sensitive kernel ($\partial C/\partial\beta$) at different depths/periods at five sites (see Ⓔ Figs. S7 and S8, electronic supplement). Based on the results, the resolution of depths is about 1500 m. According to Lin *et al.* (2009), the $S$-wave velocity of the interfaces corresponding to the top of the Pliocene formation increases from 1289 to 1703 m/s in the Western Coastal Plain. We assume that the Pliocene formation is regarded as bedrock and then the averaged $S$-wave velocity of the basement is about 1500 m/s, although the velocity contrast cannot be resolved in the study. Therefore, based on Figure 6, the depths of the Quaternary sediments are between 560 m (DIL) and 1400 m (KLU) in the Chiayi area.

Based on the gradient changes of the differential inversion results (Fig. 6), we regroup the layered structure. Furthermore, we invert the $S$-wave velocity structures at the 46 sites using stochastic inversion (Herrmann, 1991; see Ⓔ Fig. S9, electronic supplement). The shallow velocity structure (0–1000 m) can be roughly divided into 4–7 layers.

To understand variation of $S$-wave velocity in the Chiayi area, we display nine horizontal profiles of $S$-wave velocity at depths between 50 and 1500 m in Figure 7 using kriging interpolation (Cressie, 1990) based on the results of Figure 6. In terms of the results at different depths, not only is the existence of lateral heterogeneity obvious, but there are also changes in the velocity structure with depth from 270 m/s at 50 m to 2370 m/s at 1500 m. At depths of less than 1500 m, $S$-wave velocities in the eastern part of the study area are

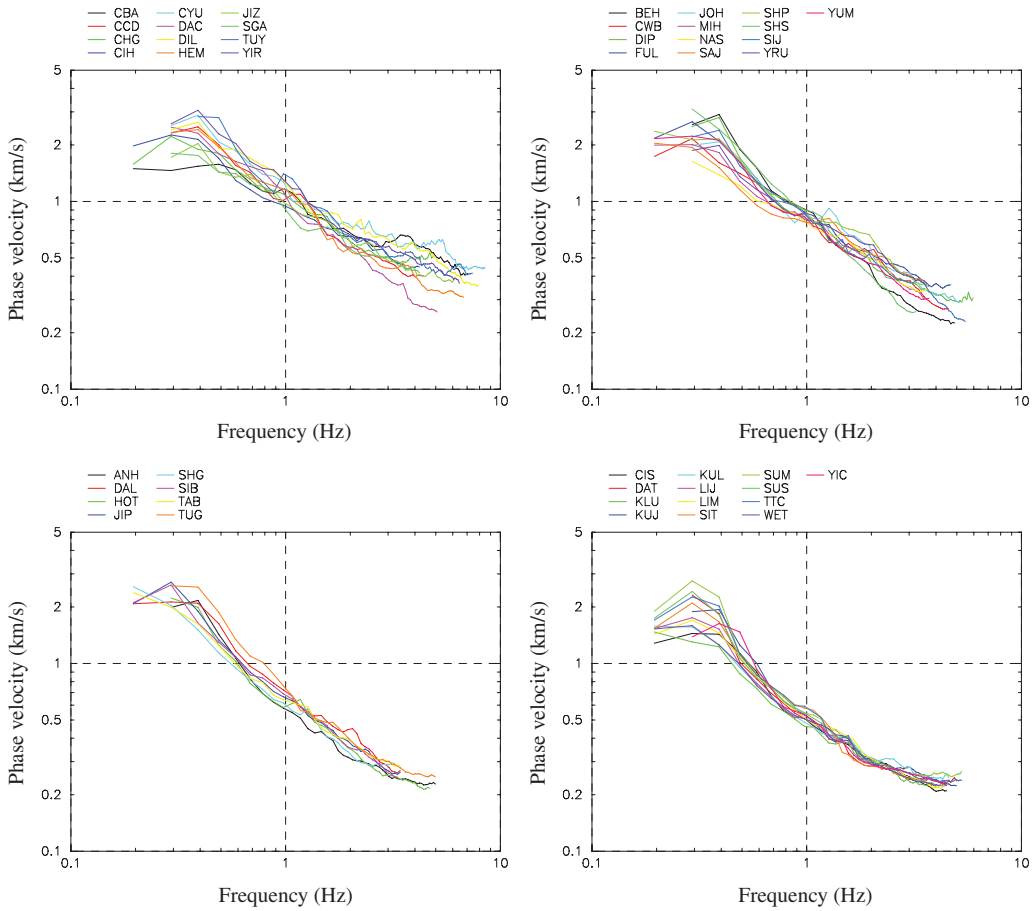


**Figure 4.** Phase velocities obtained from recordings observed at all 46 sites. They are divided into four panels for readability.

higher than those in the western part. Some features of these results are summarized below.

1. 50 m ≤ depth < 300 m: *S*-wave velocities in the whole area do not exceed 1000 m/s at depths less than 300 m. Velocities less than 330 m/s characterize the 50-m-deep soils of the western part of the study area, whereas velocities of 480–600 m/s are more characteristic of the eastern part. The northern part (CBA) of the Chiayi City has higher velocities at depths less than 200 m.
2. 300 m ≤ depth ≤ 500 m: At depths of 300–500 m, the velocity pattern is similar, but with velocities in the ranges of 560–800 and 660–1020 m/s in the west, and 920–1100 and 1050–1320 m/s in the east.
3. 500 m ≤ depth ≤ 1000 m: At depths of 500–1000 m, in addition to the eastern part, the relatively high velocities appear at some localized areas (e.g., DAT, SUM, ANH, and SHS) in the central and western parts. The *S*-wave velocities of these localized areas are between 1020 and 1230 m/s at depths of 500–700 m, and increase up to 1500 m/s at a depth of 1000 m.
4. 1000 m < depth ≤ 1500 m: At depths of 1300–1500 m, the *S*-wave velocities of the whole area are larger than 1400 m/s; especially, in the eastern part where velocities reach 2300 m/s.

Finally, based on the results of Figure 6, we use interpolation of inverse distance (Franke, 1982) to generate a 3D lattice of subsurface velocity structures beneath the Chiayi area. The lattice comprises size 250,000 nodes (i.e., $50 \times 50 \times 100$ nodes). After gridding, interpolation, and volumetric rendering, we get the 3D image of the *S*-wave velocity structures shown in Figure 8. The resolution (the distance between adjacent nodes) along with the horizontal and vertical directions of the 3D velocity model are 660 m, 923 m, and 15 m for north, east, and up–down directions, respectively. Based on the Uniform Building Code (International Conference of Building Officials (ICBO), 1997) and National Earthquake Hazard Reduction Program (Building Seismic Safety Council [BSSC], 1998), site class descriptions can be divided into six categories (A–F). Lee *et al.* (2001) only used four categories (B–E) to describe site classifications of Taiwan free-field strong-motion stations. They are type A ($V_S$ > 1500 m/s), type B (1500 m/s ≥ $V_S$ > 760 m/s), type C (760 m/s ≥ $V_S$ > 360 m/s), type D (360 m/s ≥ $V_S$ > 180 m/s), and type E ($V_S$ ≤ 180 m/s). They used average *S*-wave velocity over the upper 30 m of a site as the sole parameter for site classification. Here, we choose four velocity ranges including: 270–360, 360–760, 760–1500, and 1500–2370 m/s, because our minimum

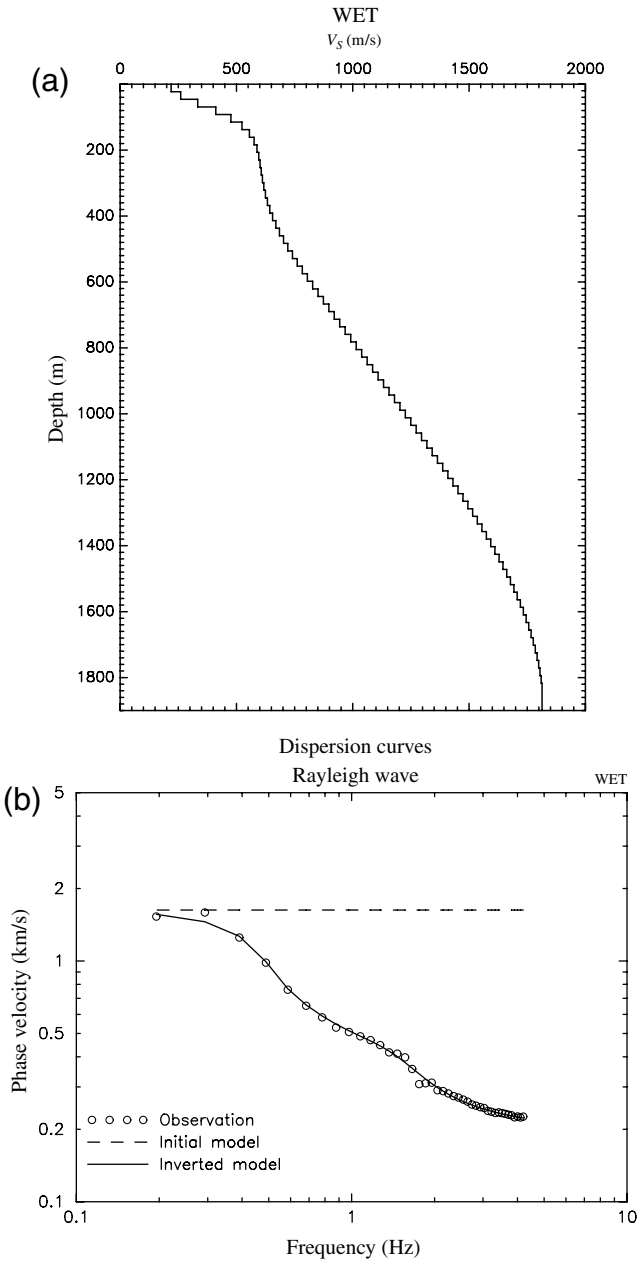


**Figure 5.** (a) Estimated *S*-wave velocity structures by differential inversion (Herrmann, 1991) at site WET. (b) Observed phase velocities (open circles) and theoretical phase velocities of the fundamental mode of the Rayleigh wave with initial (dashed line) and inverted structures (solid line).

*S*-wave velocity is 270 m/s. An overall view of the entire volume can be seen in the lower right corner of Figure 8. The 3D blocks can be rotated at any angle to understand thickness variations at different velocity intervals. From this overall view and images at velocity ranges of 270–360, 360–760, and 760–1500 m/s, we can clearly see that the thicknesses of these velocity intervals decrease from west to east. This means that the unconsolidated sediments in the western part are thicker than those in the eastern part of the study area, which may be related to the depositional environment of this area. When velocities are classified in the range of 1500–2370 m/s, variation in thickness decreases from east to west. Therefore, thickness of the sedimentary layer must increase from east to west in the Chiayi area. The final purpose to produce a 3D model of the Chiayi area is for 3D numerical simulation and ground-motion prediction in the future.

In order to examine the validity of the study, we compare our *S*-wave velocity structures with available information from geological and geophysical surveys in this area. Figure 9 shows the comparison of the *S*-wave velocity structures obtained from (a) the differential inversion technique (thick line), (b) the 30-m well-logging data (thin line), and (c) the 400-m well-logging data (open circles) at site CWB. The relative locations of these three sites are very close and the distances between them are less than 50 m. The well-logging data at two nearby sites were investigated from the surface to a depth of 30 m (Engineering Geological Database for TSMIP [EGDT]) and a depth of 400 m (Central Weather Bureau, 2009) in 2000 and 2009, respectively. At the uppermost 30 m, $V_S$ values from the 400-m well-logging data are higher than those from the 30-m well-logging data and about a factor of 3. Moreover, at depths of 30–60 m, $V_S$ values from the 400-m well-logging data are abnormally high and some of them are higher than 1000 m/s. Probably they can be attributed to some errors happening while employing well-logging method, especially at the near surface layers. At depths of 0–30 m or 0–60 m, the inversion results are similar to $V_S$ values from the 30-m well-logging data but significantly different from those from the 400-m well-logging data. Besides, the inversion results are also comparable to $V_S$ values from the 400-m well-logging data except at depths of 0–60 m and 300–400 m. The relative errors between the inversion result and $V_S$ values from the 400-m well-logging data at depths of 0–60 m, 60–300 m, and 300–400 m are about 49.9%–52%, 1.13%–23.2%, and 31.5%–45.2%, respectively.

Moreover, low velocities observed in the western part of the area mainly correspond to unconsolidated sand, silt, clay, and gravel belonging to Holocene alluvium (Chang, 2008). Relatively high velocities in the eastern part of the study area can be correlated with complicated rock mass with ages ranging from Pliocene to Pleistocene. In general, materials of clay or sand have lower electrical resistivity than hard rock, such as igneous or sedimentary rock. According to many studies (Marquis and Hyndman, 1992; Meju and Gallardo, 2003), a systematic trend exists whereby increasing velocity is associated with increasing electrical resistivity. Factors which affect electrical resistivity of soils or rocks also include porosity, water content, and grain-size distribution. In order to investigate the depositional environment in the southwestern coastal plain of Taiwan, geoelectric methods have been used in some studies (Tong, 1999; Pi, 2000; You, 2003). From horizontal slicing of electrical resistivity profiles at various depths, low electrical resistivity can be seen to exist in the western part of the Western Coastal Plain

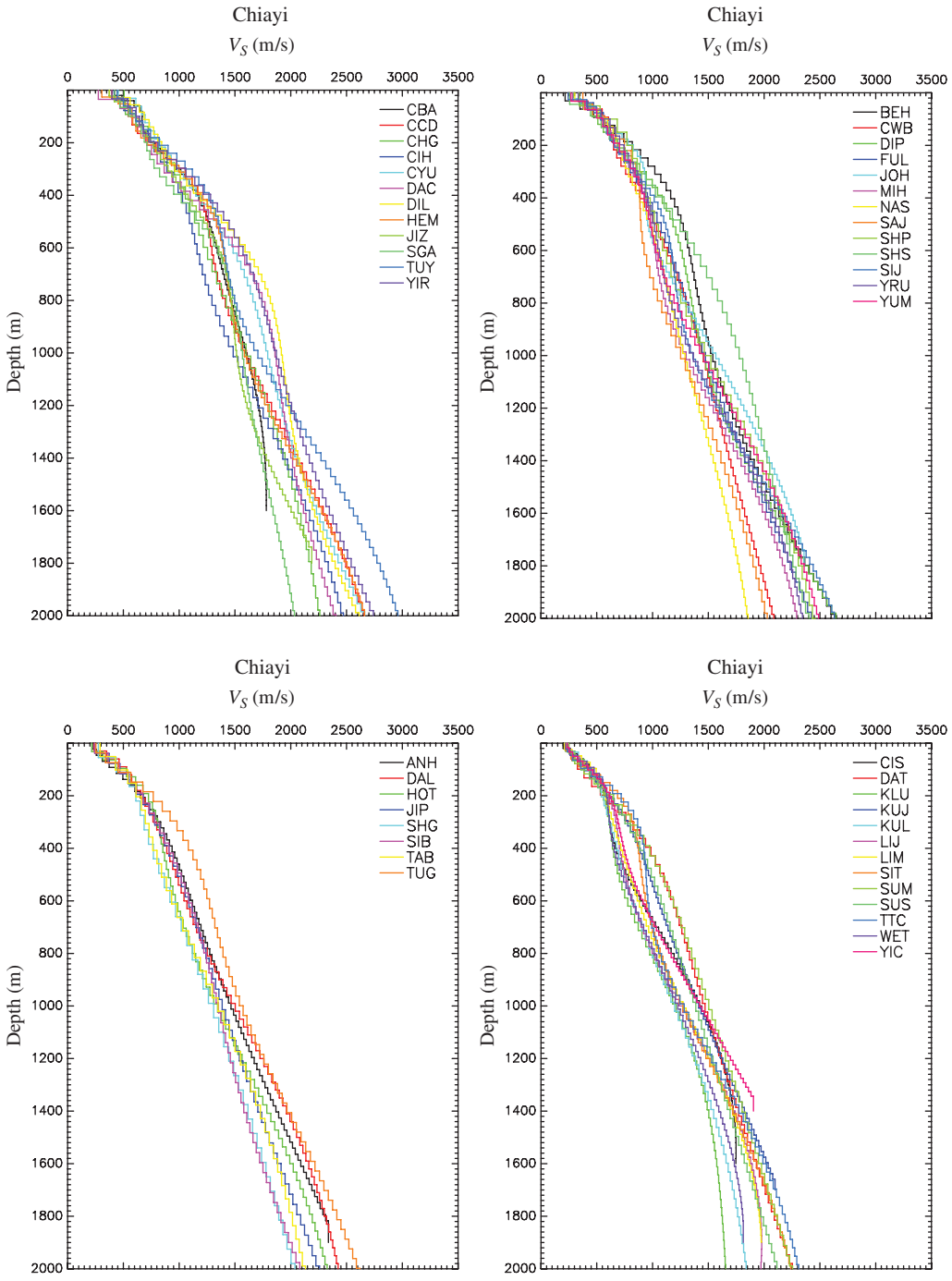


**Figure 6.** Estimated *S*-wave velocity structures by differential inversion (Herrmann, 1991) at all 46 sites. They are divided into four panels for readability.

whereas the eastern part has high electrical resistivity (see Ⓔ Figs. S10 and S11, electronic supplement). This implies that the depositional environment of the western part of the Chiayi area is within the marine facies with low electrical resistivity and consequently low velocity, whereas the eastern part of this area is of continental facies with high electrical resistivity and corresponding velocity. Besides this observation, according to the vertical electrical resistivity profile of this area, a low electrical resistivity layer extends inland from the coastline thinning gradually from west to east.

According to the above discussions, the shallow *S*-wave velocity structures in the study are in good agreement with the available geological and geophysical information of the Chiayi area. Therefore, microtremor-array measurement provides a good alternate to estimate *S*-wave velocity structures. Compared with other methods, it is easy, convenient, less

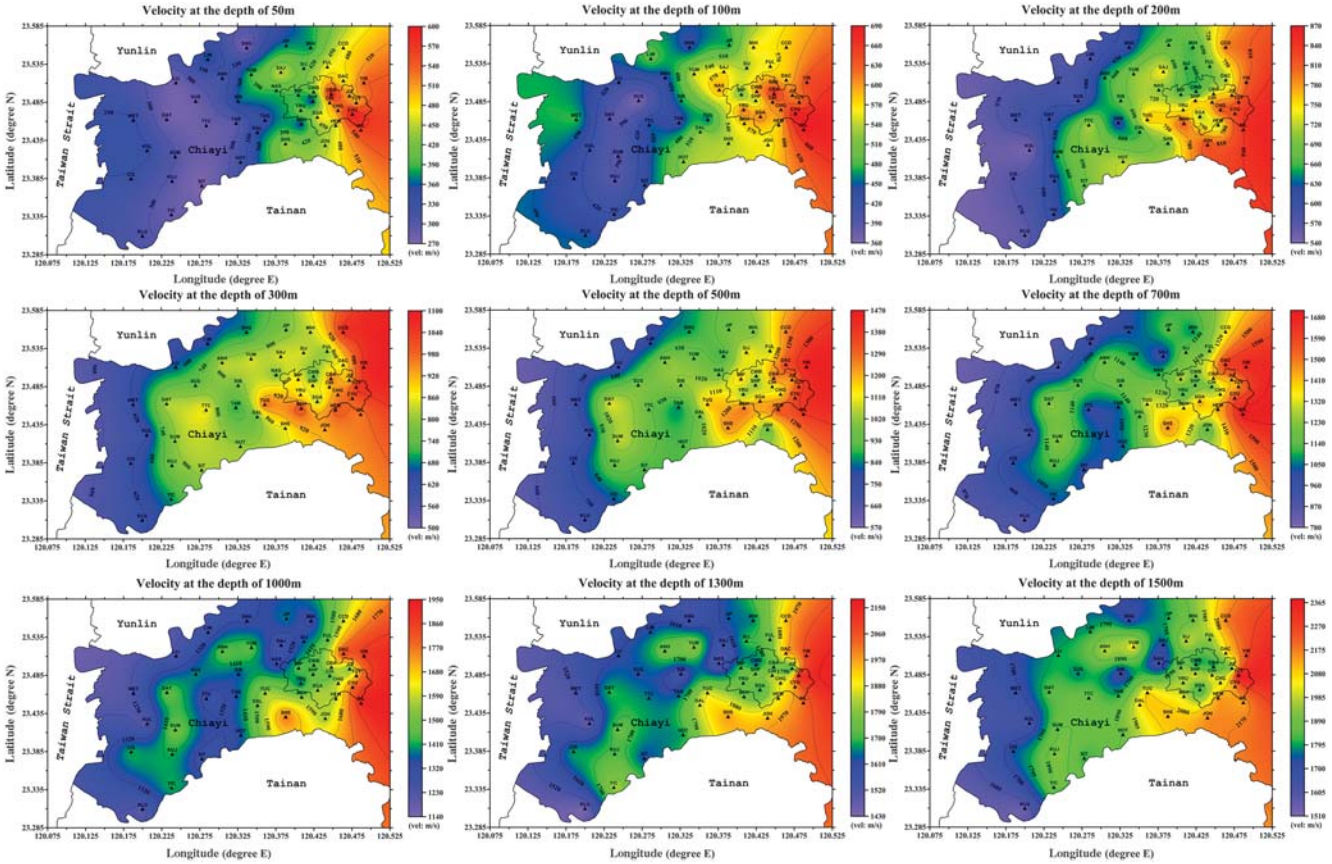


**Figure 7.** *S*-wave velocity contour maps of the Chiayi area at different depths between 50 m and 1000 m based on the results shown in Figure 6.

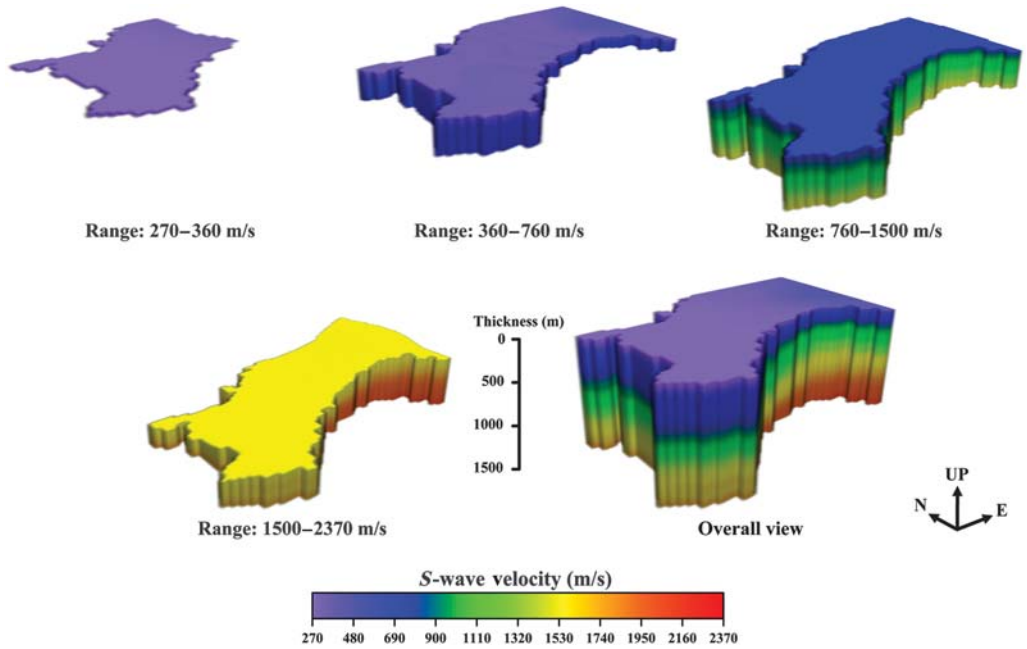


**Figure 8.** Based on Figure 6, 3D images of the Chiayi area as defined by four *S*-wave velocity ranges: 270–360, 360–760, 760–1500, and 1500–2370 m/s. The overall view of the volumetric model is exhibited in the lower right corner.

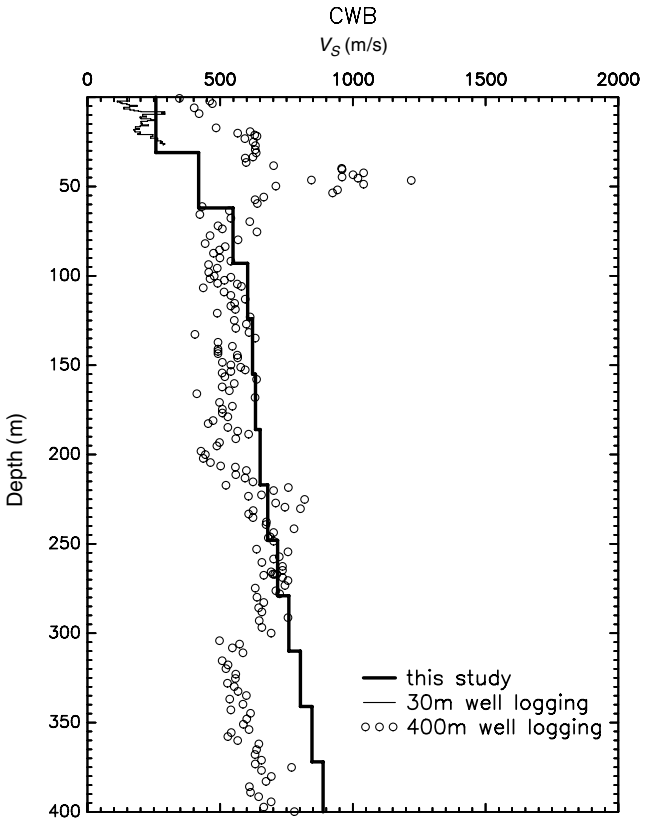


**Figure 9.** Comparison of the *S*-wave velocity structures obtained from (a) this study (thick line), (b) the 30-m well-logging data (thin line), and (c) the 400-m well-logging data (open circles) at site CWB.

expensive, and non-intrusive to obtain $V_S$ information, especially in urban areas.

## Conclusions

In this paper, the microtremor-array measurements are conducted to determine the shallow *S*-wave velocity structures of the Chiayi area. According to the previous study (known velocities for above and below the top of the Pliocene), we define the averaged *S*-wave velocity of the bedrock to be 1500 m/s although the apparent velocity contrast cannot be resolved in this case. Based on our differential inversion results, the depths of the Quaternary sediments are between 560 m (DIL) and 1400 m (KLU) in the Chiayi area. According to the stochastic inversion results, the shallow velocity structure (0–1000 m) can be roughly divided into 4–7 layers.

To understand the variations of the shallow *S*-wave velocity in the Chiayi area, we sketch 2D and 3D maps using imaging techniques based on interpolation algorithms. From the 2D results, the *S*-wave velocities in the eastern part of the area are higher than those in the western part at depths of 50–1500 m. This pattern matches well with the geological information. From the 3D results, the thickness of sediments having an *S*-wave velocity in the range 270 and 1500 m/s increases from east to west; whereas the thickness of layers having an *S*-wave velocity in the range 1500 and 2370 m/s decreases from east to west. This indicates that the thickness of unconsolidated sediments with lower *S*-wave velocities is greater in the western part than in the eastern part where higher velocities are evident. These results are consistent with the electrical resistivity distributions by the geoelectric studies (Tong, 1999; Pi, 2000; You, 2003) that show lower electrical resistivity closer to the coast representative of a thicker alluvium. This band of low electrical resistivity thins the further inland from the coast one goes, meaning the alluvium thins from west to east in the Chiayi area.

In the study, our results are in good agreement with the geological and geophysical information of the Chiayi area. Therefore, the microtremor-array measurement provides a good alternate to estimate *S*-wave velocity structures. Based on the inversion results, we can do ground-motion simulation/prediction of this area in the near future. However, the inversions have been carried out without considering the uncertainties of phase velocities of Rayleigh waves. For this reason, the uncertainties in the *S*-wave velocity models are not estimated, and the 3D *S*-wave velocity model must be used with caution while doing earthquake-scenario simulations.

## Data and Resources

The 30-m well-logging data were obtained from Engineering Geological Database for TSMIP (EGDT; http://egdt.ncree.org.tw/, last accessed September 2012). The 400-m well-logging data were provided by Taiwan Central Weather Bureau and are proprietary. Microtremor data used in this study were collected by the Engineering Seismology Laboratory, National Chung Cheng University, Taiwan.

## Acknowledgments

We would like to express our gratitude to R. D. Hwang for his stimulating discussions. We appreciate the efforts of the Engineering Seismology Laboratory of National Chung Cheng University, which provided microtremor-array measurements in the field. We also wish to thank S. Parolai, M. Asten, and one anonymous reviewer for their valuable comments and suggestions to improve this article. We also thank Taiwan Central Weather Bureau and L. T. Tong for providing the well-logging data and electrical resistivity data, respectively. The National Science Council, Taiwan, has supported this research (NSC 96-2119-M-194-001).

## References

Asten, M. W., and J. D. Henstridge (1984). Array estimator and the use of microseisms for reconnaissance of sedimentary basins, *Geophysics* **49,** 1828–1837.

Building Seismic Safety Council (BSSC) (1998). 1997 Edition NEHRP Recommended Provisions for Seismic Regulations for New Buildings and Other Structures, FEMA 302/303, Part 1 (Provisions) and Part 2 (Commentary), developed for the Federal Emergency Management Agency, Washington, D.C., 337 pp.

Capon, J. (1969). High-resolution frequency–wavenumber spectral analysis, *Proc. IEEE* **57,** 1408–1419.

Central Geology Survey (2010). Integrated Geological Data Inquiry System, Central Geology Survey, the Ministry of Economic Affairs, Taipei,

Taiwan, http://gis.moeacgs.gov.tw/gwh/gsb97-1/sys8/index.cfm (last accessed in September 2012).

Central Weather Bureau (2009). The final report for the deployments of the well and the station building of downhole seismometers in 2009, Central Weather Bureau, Ministry of Transportation and Communications, Taipei, Taiwan (in Chinese), 32 pp.

Chang, H. C. (2008). Explanatory text for the geological map of Taiwan (Chiayi, scale 1:50,000, sheet 44), Central Geology Survey, the Ministry of Economic Affairs, Taipei, Taiwan (in Chinese with English abstract), 81 pp.

Chung, J. K., and Y. T. Yeh (1997). Shallow crustal structure from short-period Rayleigh-wave dispersion data in southwestern Taiwan, *Bull. Seismol. Soc. Am.* **87,** 370–382.

Cressie, N. (1990). The origins of Kriging, *Math. Geol.* **22,** 239–252.

Dutta, U., T. Satoh, T. Kawase, T. Sato, N. Biswas, A. Martirosyan, and M. Dravinski (2007). *S*-wave velocity structure of sediments in Anchorage, Alaska, estimated with array measurements of microtremors, *Bull. Seismol. Soc. Am.* **97,** 234–255.

Franke, R. (1982). Scattered data interpolation: Test of some methods, *Math. Comp.* **33,** 181–200.

Herrmann, R. B. (1987). *Computer Programs in Seismology*, University of St. Louis, Missouri, 104 pp.

Herrmann, R. B. (1991). *Computer Programs in Seismology, Vol. IV: Surface Wave Inversion*, University of St. Louis, Missouri, 58 pp.

Ho, C. S. (1982). *Tectonic Evolution of Taiwan: Explanatory Text of the Tectonic Map of Taiwan*, the Ministry of Economic Affairs, Taipei, Taiwan (in Chinese), 153 pp.

Horike, M. (1985). Inversion of phase velocity of long-period microtremors to the *S*-wave-velocity structure down to the basement in urbanized area, *J. Phys. Earth* **33,** 59–96.

Huang, H. C., and C. F. Wu (2006). Estimation of *S*-wave velocity structures in the Chiayi City, Taiwan using array records of Microtremors, *Earth Planets Space* **58,** 1455–1462.

Hwang, R. D., G. K. Yu, W. Y. Chang, and J. P. Chang (2003). Lateral variations shallow shear-velocity structure in southwestern Taiwan inferred from short-period Rayleigh waves, *Earth Planets Space* **55,** 349–354.

International Conference of Building Officials (ICBO) (1997). *Uniform Building Code*, Whittier, California, 492 pp.

Lee, C. T., C. T. Cheng, C. W. Liao, and Y. B. Tsai (2001). Site classification of Taiwan free-field strong-motion stations, *Bull. Seismol. Soc. Am.* **91,** 1283–1297.

Lin, C. M., T. M. Chang, Y. C. Huang, H. J. Chiang, C. H. Kuo, and K. L. Wen (2009). Shallow *S*-wave velocity structures in the Western Coastal Plain of Taiwan, *Terr. Atmos. Ocean. Sci.* **20,** 299–308.

Marquis, G., and R. D. Hyndman (1992). Geophysical support for aqueous fluids in the deep crust: Seismic and electrical relationships, *Geophys. J. Int.* **110,** 91–105.

Meju, M. A., and L. A. Gallardo (2003). Evidence for correlation of electrical resistivity and seismic velocity in heterogeneous near-surface materials, *Geophys. Res. Lett.* **30,** 1373–1376.

Menke, W. (1984). *Geophysical Data Analysis: Discrete Inversion Theory*, Elsevier, New York, 260 pp.

Mundepi, A. K., J. J. Galiana-Merino, Kamal, and Conrad Lindholm (2010). Soil characteristics and site effect assessment in the city of Delhi (India) using H/V and $f$–$k$ methods, *Soil Dynam. Earthq. Eng.* **30,** 591–599.

Pi, H. W. (2000). A study of the stratum boundary between late Pleistocene and Holocene in Coastal Plain, southwestern Taiwan by direct current resistivity method, *Master's dissertation*, National Central University, Chung-Li, Taiwan (in Chinese with English abstract), 87 pp.

Picozzi, M., A. Strollo, S. Parolai, E. Durukal, O. Özel, S. Karabulut, J. Zschau, and M. Erdik (2009). Site characterization by seismic noise in Istanbul, Turkey, *Soil Dynam. Earthq. Eng.* **29,** 469–482.

Pilz, M., S. Parolai, M. Picozzi, R. Wang, F. Leyton, J. Campos, and J. Zschau (2010). Shear wave velocity model of the Santiago de Chile basin derived from ambient noise measurements: a comparison of proxies for seismic site conditions and amplification, *Geophys. J. Int.* **182,** 355–367.

Pilz, M., S. Parolai, M. Stupazzini, R. Paolucci, and J. Zschau (2011). Modelling basin effects on earthquake ground motion in the Santiago de Chile basin by a spectral element code, *Geophys. J. Int.* **187,** 929–945.

Satoh, T., H. Kawase, and S. Matsushima (2001). Estimation of *S*-wave velocity structures in and around the Sendai basin, Japan, using array records of microtremors, *Bull. Seismol. Soc. Am.* **91,** 206–218.

Tong, L. T. (1999). Annual report on hydrogeological survey of the groundwater monitoring network in Taiwan (II): Geophysical surveys and stratigraphic correlation in the Chianan Plain, Central Geology Survey, the Ministry of Economic Affairs, Taipei, Taiwan (in Chinese), 122 pp.

Wen, S., and C. H. Chen (2004). 3-D velocity structure beneath the Chia-Nan Area, Taiwan, *Terr. Atmos. Ocean. Sci.* **15,** 239–259.

You, J. I. (2003). Using DC resistivity and CSAMT methods for studying the changes of depositional environment in the southwestern coastal plain of Taiwan, *Ph.D. dissertation*, National Central University, Chung-Li, Taiwan (in Chinese with English abstract), 157 pp.

Department of Earth and Environmental Sciences
National Chung Cheng University
No. 168, Sec. 1, University Rd.
Min-Hsiung Township, Chiayi County 621
Taiwan, R. O. C.
seihuey@eq.ccu.edu.tw (H.C.H)

Manuscript received 5 September 2011